

## **Feature of the flow over a finite length square cylinder on a wall at various incidence angles**

A. Sohankar<sup>1)</sup>, M. Kazemi Esfeh<sup>2)</sup>, H. Pourjafari<sup>3)</sup>, Md. Mahbub Alam<sup>4)</sup>,  
\*Longjun Wang<sup>5)</sup>

<sup>1,2)</sup> *Mechanical Engineering Department, Isfahan University of Technology, Isfahan, Iran*

<sup>3)</sup> *Mechanical Engineering Department, Yazd University, Yazd, Iran*

<sup>4,5)</sup> *Institute for Turbulence-Noise-Vibration Interaction and Control, Shenzhen Graduate School, Harbin Institute of Technology, Shenzhen 518055, China*

### **ABSTRACT**

Wake characteristics of the flow over a finite square prism at different incidence angles were experimentally investigated using an open-loop wind tunnel. A finite square prism with a width  $D=15$  mm and a height  $H=7D$  was vertically mounted on a horizontal flat plate. The Reynolds number is varied from  $6.5 \times 10^3$  to  $28.5 \times 10^3$  and the incidence angle  $\alpha$  is adjusted from  $0^\circ$  to  $45^\circ$ . The ratio of boundary layer thickness to the prism height was about  $\delta/H=7\%$ . The time-averaged velocity, turbulence intensity and the vortex shedding frequency were obtained through a single-component hot-wire probe. Power spectrum of the streamwise velocity fluctuations revealed that the tip and base vortices shed at the same frequency as that of spanwise vortices. Furthermore, the results showed that the critical incidence angle associated with the maximum Strouhal number and minimum wake width, occurred at  $\alpha_{cr} = 15^\circ$  which is equal to that reported for an infinite prism. There is a reduction in the size of the wake region along the height of the prism when moving away from the ground plane towards the free end.

**Keywords:** experimental study; finite square prism; incidence angle; low-speed wind tunnel; hot-wire; Strouhal number

### **Nomenclature**

Latin symbols

$D$  Side length of the prism  
 $D'$  Projected width of the prism  
 $f$  Frequency  
 $H$  Height of the prism

---

<sup>1</sup> Associate Professor

<sup>2,5</sup> PhD Student

<sup>3</sup> MSc

<sup>4</sup> Professor

$Re$  Reynolds number  
 $U$  Free stream velocity  
 $U(y)$  Inlet mean flow velocity profile  
 $u$  Time-averaged (mean) velocity  
 $u_{rms}$  Root-mean-square of the fluctuating velocity  
 $TI \%$  Turbulence intensity  
 $St$  Strouhal number based on  $D$   
 $St'$  Strouhal number based on  $D'$   
 $W$  Wake width  
 $X$  Streamwise coordinate  
 $Y$  Wall-normal coordinate  
 $Z$  Crossstream coordinate

#### Greek Symbols

$\alpha$  Incidence angle  
 $\alpha_{cr}$  Critical incidence angle  
 $\delta$  Boundary layer thickness

## 1. INTRODUCTION

As one of the most important research topics of bluff-body aerodynamics, the flow around infinite or two-dimensional square prisms has been widely investigated both numerically and experimentally over the years (Lee 1975; Igarashi 1984; Norberg 1993; Lyn et al. 1995; Williamson 1996; Sohankar et al. 1999, 2000; Duta et al. 2003; Sohankar 2006, 2008; Brun et al. 2008; Minguéz et al. 2011; Alam et al. 2011; Yen et al. 2011; Trias et al. 2015; Alam et al. 2016, Zheng and Alam 2017). Many engineering applications, however, involve the flow around surface-mounted finite-height bluff bodies, such as buildings, bridges and bridge supports and power station smokestacks. The flow around such surface-mounted finite-height prisms is highly three-dimensional due to the end effects (resulting in tip and base vortices) and spanwise vortices. Fig. 1(a) shows a schematic of the flow around a surface-mounted finite-height square prism of side length  $D$ , and height  $H$ . In this figure,  $X$ ,  $Y$  and  $Z$  are the coordinate axes in the streamwise, wall-normal and cross-stream directions, respectively. Here, the prism is mounted normal to a ground plane and is partially immersed in the flat-plate boundary layer, where  $U(y)$  is the incoming mean flow velocity profile,  $U$  is the freestream velocity outside the boundary layer on the ground plane, and  $\delta$  is the boundary layer thickness. For such a body, the flow field is influenced by the flow around the free end and the flow around the prism ground plane junction, and then the local flow field becomes strongly three-dimensional.

The turbulent flow around a finite square prism has received far less attention than the flow around an infinite prism because of its complexity. The Karman vortex shedding from the sides, the streamwise tip vortices and its induced downwash flow, a pair of base vortices near the ground plane and its upwash flow, the horseshoe vortex at the junction between the prism and the ground plane are main factors for the complex wake structure of this type of body (Fig. 1(b)).

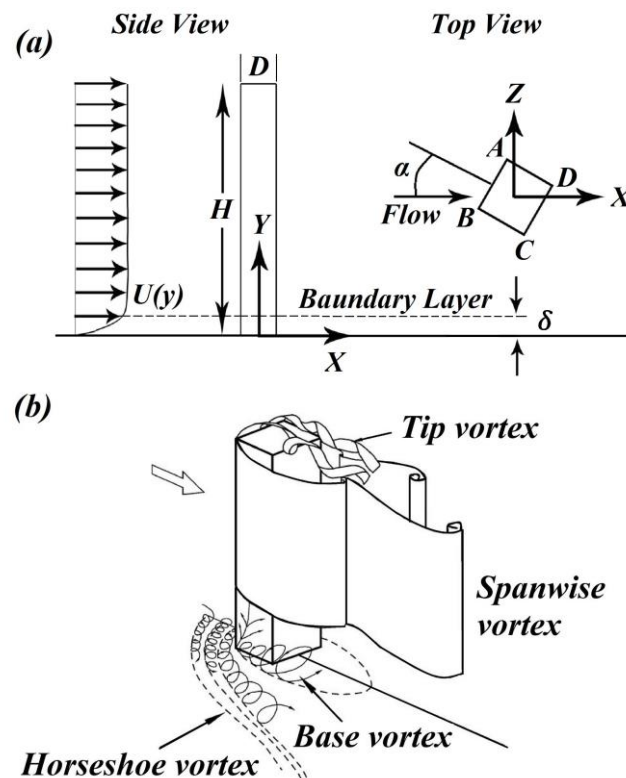


Fig. 1 Schematic of a finite square prism mounted normal to a ground plane: (a) side and top views (b) flow structure around a wall-mounted finite-length square cylinder (Wang and Zhou 2009)

## 2. LITERATURE REVIEW

### 2.1 Infinite square prism at incidence

As the incidence angle is changed from  $\alpha=0^\circ$  to  $45^\circ$ , there are variations in time-mean drag coefficient  $C_D$  and Strouhal number  $St$ , and the prism begins to experience a non-zero mean lift coefficient  $C_L$  (McClellan and Sumner 2014). The main reasons for aforementioned variations are the changes on the flow separation positions and the differences in the shear layers emanating from the two sides of the prism. The other possible reasons are the flow reattachment on one of the side surfaces, the proximity effects of the rear corner on the interactions between the shear layers, changes in the wake width, and the vortex formation length or location of shear layer roll-up (Duta et al. 2003, Igarashi 1984, Norberg 1993, Sohankar 2006, 2008), Wang and Zhou 2009, Adaromola et al. 2006).

Huang et al. (2010) used smoke flow visualization, surface-oil flow technique, and the resultant flow topology to identify three flow structure modes exhibited by an infinite square prism at  $Re=3.4 \times 10^4 - 9.4 \times 10^4$ , and  $\alpha = 0^\circ - 45^\circ$ . They classified the flow patterns as “subcritical flow”, where there is no reattachment of the separated shear layer onto the lower surface ( $\alpha < \alpha_{cr}$ ), “supercritical flow”, where a separation bubble occurs on the lower surface ( $\alpha > \alpha_{cr}$ ), and “wedge flow” ( $\alpha = 45^\circ$ ). In addition, they

reported that the minimum wake width occurs at  $\alpha = \alpha_{cr}$ . Sohankar et al. (2015) also reported similar findings for  $Re = 2 \times 10^3 - 8 \times 10^3$  via smoke flow visualization. At  $\alpha = \alpha_{cr}$ ,  $C_D$  and  $C_L$  attain a minimum value, and  $St$  achieves a maximum value. The  $\alpha_{cr}$  is sensitive to  $Re$  and free stream turbulence intensity (Chen and Liu 1999, Huang et al. 2010, Lee 1975, Sohankar et al. 2015). For a low freestream turbulence intensity,  $\alpha_{cr}$  lies between  $11^\circ$  to  $15^\circ$ . For  $Re = 2 \times 10^3 - 4 \times 10^3$ ,  $\alpha_{cr} = 17^\circ$  has also been reported (Chen and Liu 1999).

## **2.2 Finite square prism**

The boundary layer thickness and  $\alpha$  as well as the prism aspect ratio  $AR (= H/D)$  are some of the parameters that influence the flow field of a finite square prism. The following section demonstrates briefly some of the main flow features of the finite square prisms.

**End effects:** The free end of a finite-height cylinder is one of the main sources of the three-dimensionality of the flow. The free end alters the vortex formation region, vortex-shedding pattern and the surface pressure distribution (Yen and Yang 2012). The free end creates tip vortices, which induces a downward-directed velocity field along the cylinder height known as the downwash flow (Adaramola et al. 2006). Around the junction of the cylinder with the ground-plane, an adverse pressure gradient is produced. Consequently, the boundary layer is forced to separate from the ground-plane and ultimately a horseshoe vortex is formed wrapping around the base of the cylinder. These vortices carry on moving with the stream towards the downstream (Park and Lee 2000). According to Okamoto and Sunabashiri (1992), the size of the horseshoe vortex decays with increasing  $H$ .

**Aspect ratio effect:** From the literature (Okamoto and Sunabashiri 1992, Adaramola et al. 2006), the finite cylinders of small  $AR$  (less than the “critical  $AR$ ”) have a wake structure different from those of higher  $AR$ . For finite cylinders greater than the critical  $AR$ , the flow pattern is characterized by the presence of the anti-symmetric Kármán vortex shedding, whereas, for cylinders less than the critical  $AR$ , the wake structure is often described as symmetric “arch vortex shedding”. Adaramola et al. (2006) and Sumner et al. (2009) suggested that the critical  $AR$  of a finite circular cylinder lies between  $AR = 3$  and  $5$ . For a finite square prism, McClean and Sumner (2014) also suggested that the critical  $AR$  is between  $AR=3$  and  $5$ , under similar conditions. Wang et al. (2004) studied the flow over a surface-mounted finite-height square cylinder of  $AR = 3 - 7$ . A broad-banded peak in the power spectrum at  $St = 0.09$  was obtained for  $AR=3$ , while for  $AR=5$  and  $7$ , pronounced sharp peaks at  $St=0.12$  and  $0.13$  were observed, respectively. For an infinite square cylinder,  $St = 0.135$  was reported.

**Boundary layer thickness effect:** Studies show that besides  $AR$ ,  $\delta$  affects the creation of the base vortices and formation of the upwash flow. Where a thicker boundary layer is present, the base vortices are stronger and the upwash flow is more effective. The presence of a stronger upwash flow also affects the free end region as it prevents the downwash flow to reach the ground plane and results in weaker tip

vortices (Wang et al. 2006). Sakamoto and Arie (1983) investigated that with increasing  $\delta$ ,  $St$  decreases for all rectangular prisms.

Wang et al. (2006) studied the effect of  $\delta$  on the flow around a finite square cylinder of  $AR=5$ . They showed that  $\delta$  has a significant effect on the creation and the size of the base vortices. -Both symmetric and anti-symmetric vortices are identified in the near wake region of the wall-mounted square cylinder for a given  $AR$ . The probability of anti-symmetrical vortex shedding varies with aspect ratio and the boundary layer thickness. The probability of anti-symmetrical vortex shedding considerably increases with increasing the boundary layer thickness, particularly near the base of the cylinder.

**Incidence angle effect:** Sarode et al. (1981) measured  $C_D$  and  $C_L$  for surface-mounted finite-height square prisms of  $AR=1.14$  to  $10$  at  $Re = 2.2 \times 10^4$ . The prisms were immersed in an atmospheric boundary layer. They found that  $\alpha$  effects on  $C_D$  were significant for the more slender prisms, i.e., at  $AR=6.36$  and  $10$ , while for the smaller  $AR$  ( $=1.14, 2.27$ , and  $3.64$ ),  $\alpha$  effects on  $C_D$  were much less significant. In addition, as  $AR$  decreases,  $C_L$  reduced in magnitude (Sarode et al. 1981).

McClellan and Sumner (2014) at  $Re = 7.2 \times 10^4$  investigated the effects of  $AR$  ( $= 3 - 11$ ) and  $\alpha$  ( $=0^\circ - 45^\circ$ ) on  $C_D$ ,  $C_L$  and  $St$  for a surface-mounted finite square prism.  $C_D$ ,  $C_L$ , and  $St$  are found to be very sensitive to  $\alpha$ . This is similar to what was observed for infinite square prisms. For all  $AR$  – tested,  $\alpha_{cr}$  associated with the minimum  $C_D$ , maximum  $C_L$  (magnitude), and maximum  $St$ , was  $15^\circ - 18^\circ$ , higher than the typical  $\alpha_{cr}$  range for infinite square prisms.

There are limited studies on the turbulent wake of a finite square prism. Therefore, there is a need for further studies that would provide more insight into the turbulent wake of these structures. This study aims to investigate experimentally the flow around a wall-mounted finite-height square prism at a non-zero angle of incidence in order to gain a better understanding of the main feature of flow structure, particularly, the effect of incidence angle on the vortex shedding. The authors provide new information on the Strouhal number data in order to extend the result of earlier studies (Sarode et al. 1981; Sakamoto 1985; McClellan & Sumner 2014). To find the flow field features over a finite-height square prism, the turbulent wake structure including time-averaged velocity and turbulence intensity was studied extensively at different incidence angles, using the data extracted from a hot-wire anemometry. The experiments, performed in a wind tunnel, cover a relatively wide range of  $Re = 6.5 \times 10^3 - 28.5 \times 10^3$  and of  $\alpha = 0^\circ - 45^\circ$  for  $AR=7$ .

### 3. EXPERIMENTAL SET-UP

Flow measurements were performed in an open return wind tunnel with a test section height, width and length of  $46, 46$  and  $120$  cm, respectively. The section's sidewalls are made of Plexiglas thereby aiding the visualization of the experimental apparatus. The maximum empty test section speed of this wind tunnel is approximately  $30$  m/s. The contraction ratio between the settling chamber and test section is  $5:1$ . A honeycomb and three turbulence reduction screens are located at the inlet-settling chamber to reduce tunnel turbulence to less than  $0.3\%$  in the test section. The velocity non-uniformity outside the test-section wall boundary layers was less than  $1.5\%$  over



the speed range of the present experiments. The free stream turbulent was less than 0.3% in the speed range examined.

A smooth steel square prism of a width  $D = 15$  mm and an aspect ratio  $AR = 7$  was used throughout the experiments. The square prism had sharp edges on all sides. The blockage ratio (the ratio of the frontal area of the prism to the cross-sectional area of the test section) ranges from 0.7% (for  $\alpha = 0^\circ$ ) to 1.1% (for  $\alpha = 45^\circ$ ) and hence the wind tunnel walls effects on the measured quantities can be negligible (McClean and Sumner 2014, West and Apelt 1982).

The wind tunnel test section is equipped with a three-axis traverse system, which is controlled by a LabVIEW computer program. This traverse system is mounted above the wind tunnel such that the hot-wire probe supporting structure enters the wind tunnel from the ceiling as shown in Fig. 2. Three step motors are used in the traversing mechanism to control the vertical and horizontal position of the measurement probe of the hot-wire system with the accuracy of  $\pm 0.1$  mm.



Fig. 2. wind tunnel test section and traverse mechanism.

The time-mean and fluctuating streamwise velocities were measured using a single hot-wire probe. The probe was calibrated both statically and dynamically and all data were low-pass filtered. Data were recorded via a 12-bit A/D. In order to quantify the uncertainty of the hot-wire anemometer, the methodology provided in (Jorgenson 2002, Yavuzkurt 1984) were followed. The uncertainty of the results obtained with the CTA anemometer is a combination of the uncertainties of the individually acquired voltages converted into velocity. The uncertainty of each individual velocity sample was determined by non-statistical means based on detailed knowledge of the instrumentation, calibration and experimental conditions. The hot-wire anemometer has a negligible drift, low noise, and good repeatability so that these factors do not add significantly to the uncertainty in comparison with other error sources (Jorgenson 20052). The uncertainties of the time-average velocity and turbulence intensity (TI) were found to be around 3.6% and 6%, respectively.

Measurements of the boundary layer velocity profiles and properties were made using a single hot-wire probe at a free-stream velocity of  $U_0=20$  m/s. The time-averaged streamwise velocity and turbulence intensity profiles of the ground plane boundary layer at the location of the prism (with the prism removed) are shown in Fig. 3. The boundary layer thickness is  $\delta=7.5$  mm at the prism location (Fig. 3). This boundary layer provides a thickness-to-side-length ratio of  $\delta/D=0.5$  and a thickness-to-height ratio of  $\delta/H=0.07$ . The boundary layer thickness may have a pronounced influence on the flow structure around a wall-mounted finite-length cylinder (Wang and Zhou 2009). It is noted that in the present study the boundary layer thickness is approximately  $\delta=7.5$  mm (or  $\delta/H=7\%$ ) for freestream velocity of  $U_0=20$  m/s, which is negligibly small when compared with the height of the square prism. Therefore, the effect of boundary layer thickness on the wake structure can be neglected.

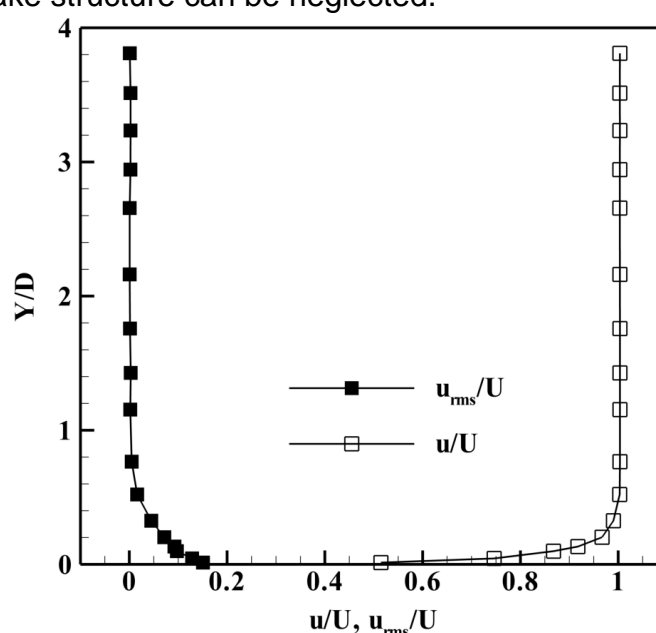


Fig. 3. Time-averaged streamwise velocity and turbulence intensity profiles of the ground plane boundary layer of wind tunnel. Measurements were performed in the absence of cylinder.

## 4. RESULTS AND DISCUSSION

The results of this study will be presented in two subsections including mean flow field and Strouhal number.

### 4.1 Mean flow field

One of the characteristics of a finite prism is that the wake structure changes significantly from the tip to the base of the prism. Fig. 4 presents the time-averaged velocity profiles at  $\alpha=0^\circ$  along the spanwise direction for various  $Y/D$  at  $X/D=3$ ,  $Re=2 \times 10^4$ . It should be noted that the origin of the coordinate system is at the cylinder center on the wall, see Fig. 1. It is seen that the velocity profiles for  $Y/D = 3.5 - 6.5$  have two peaks with low values in the region of about  $1.5 < Z/D < 1.5$ , where the value of this minimum velocity increases with  $Y/D$ . The appearance of two peaks in some  $Y/D$  is due to the effect of downwash flow from the free end as reported by Adaramola et al.

(2006) and Okamoto and Sunabashiri (1992). In other words, the downwash flow, which originates from the prism's free end and descends into the wake, extends to the mid-height of the square prism and therefore the wake flow is divided into two similar regions. This is a reason for providing two peaks in the time-averaged velocity profiles in Figs. 4. It seems that near the ground plane ( $Y/D=0.5$  and  $1.5$ ) the time-averaged velocity profiles have only a single peak. This is due to the fact that flow field close to the ground plane ( $Y/D<3.5$ ) is not influenced by the downwash flow. Fig. 4 also shows that the velocity at the mid-span ( $Z/D=0$ ) increases from about 0.2 to 1 close to the wall ( $Y/D=0.5$ ) and ceiling ( $Y/D=7$ ), respectively.

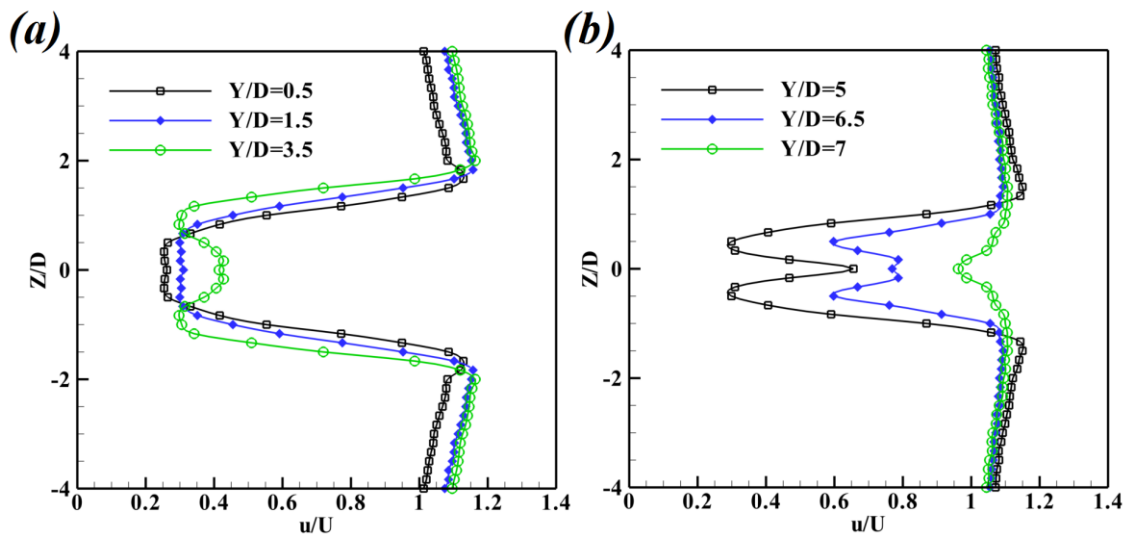


Fig. 4. The time-average velocity profiles along the spanwise direction ( $Z$ ) at various heights ( $Y/D=0.5-7$ ,  $\alpha=0^\circ$  and  $Re=2 \times 10^4$ ,  $X/D=3$ ): (a) lower half of the prism, (b) upper half of the prism.

Fig. 5 presents the time-averaged velocity profile at three different incidence angles ( $\alpha=0^\circ$ ,  $15^\circ$ ,  $45^\circ$ ) along the streamwise direction ( $X/D=3, 5$ ) at mid-height of the square prism. At  $X/D=3$  all velocity profiles have two peaks (Fig. 5(a)). As mentioned before these peaks originate from the downwash flow from the free end surface. It seems that at  $X/D=5$ , the downwash flow does not reach the mid-section ( $Y/D=3.5$ ) at  $\alpha=15^\circ$  and the time-averaged velocity profiles have only a single peak (Fig. 5(b)).

Fig. 6 presents the time-average velocity profiles in the wake region on the  $XY$  plane at the wake centerline ( $Z/D=0$ ) for  $\alpha=0^\circ$  and  $45^\circ$  ( $Re=20000$ ). Although velocity profiles are roughly similar in two cases for  $X/D=5, 7.5$  and  $10$ , but at  $X/D=3$  the velocity profiles are markedly different from each other. As seen from Fig. 6, at  $X/D=3$ , the velocity profiles have relatively large variation near the free end of the cylinder ( $Y/D=7$ ), where a strong separating free shear layer forms. This shear layer flow provides a downwash flow behind the cylinder. Fig. 6 reveals that separating shear layer and the corresponding large velocity gradient near the free-end surface are more notable for  $\alpha=45^\circ$  than for  $\alpha=0^\circ$ .



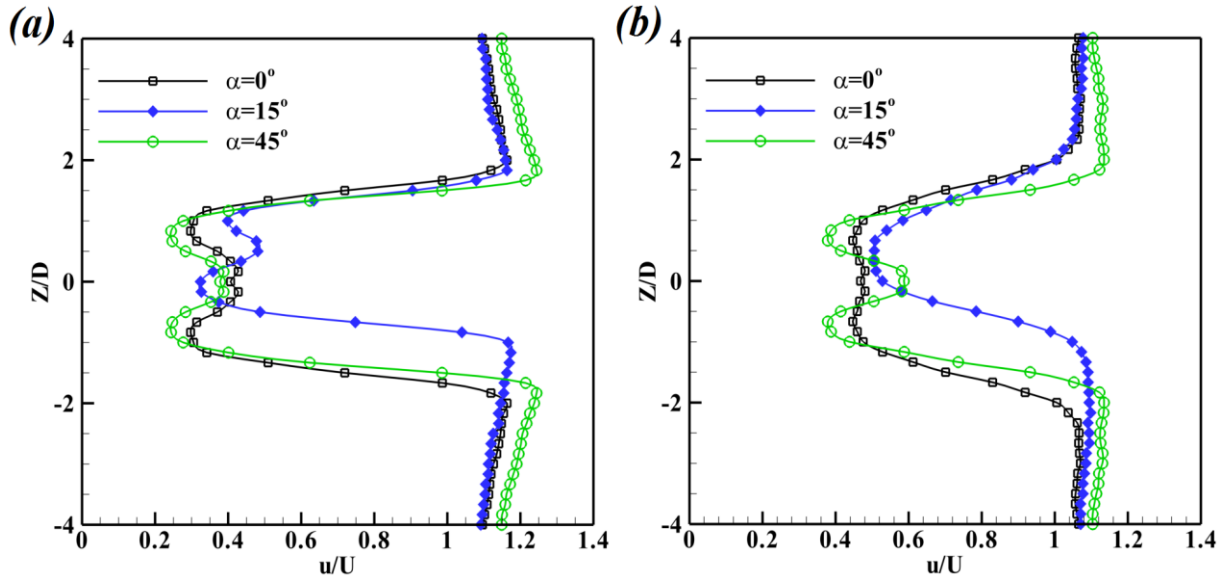


Fig. 5. Mean velocity profiles along the spanwise direction ( $Z$ ) at various angles ( $Y/D=3.5$  and  $Re=2 \times 10^4$ ): (a)  $X/D=3$ , (b)  $X/D=5$ .

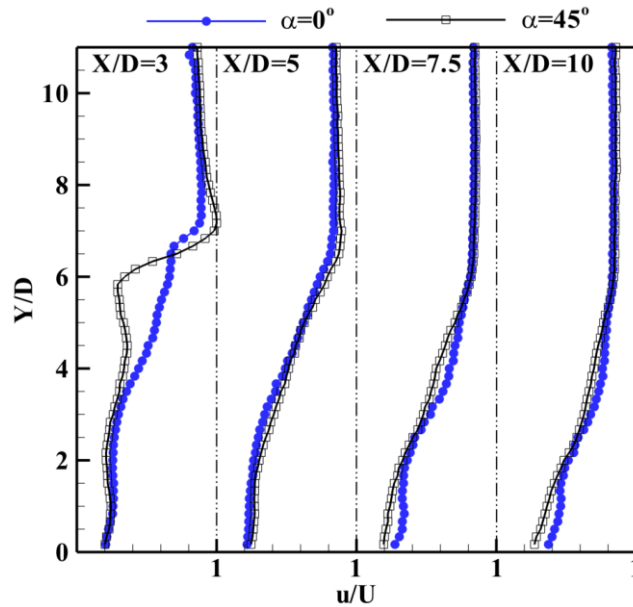


Fig. 6. Time-average velocity profiles on the  $XY$  plane at wake center plane ( $Z/D=0$ ), ( $Re=2 \times 10^4$ ,  $\alpha=0^\circ, 45^\circ$ )

Turbulence intensity (the root-mean-square of the fluctuating velocity) contours for  $\alpha=0^\circ-45^\circ$  are presented in Fig. 7. They are scaled with the free stream velocity. In general, the turbulence intensity increases in the wake region with an increase in  $X/D$  attaining a maximum at  $3 < X/D < 8$  before decaying. The turbulence structure experiences substantial changes with increasing  $\alpha$ . The turbulence intensity is symmetric with respect to the wake center ( $Z/D=0$ ) at  $\alpha=0^\circ$ . With increasing  $\alpha$  from  $\alpha=0^\circ$  to  $15^\circ$ , the asymmetry in the turbulence structure grows. The asymmetry is alleviated with a further increase in  $\alpha$ , turbulence structure eventually becoming

symmetric at  $\alpha=45^\circ$ . It should be noted that the turbulent wake of a finite square prism is dramatically different from an infinite square prism. Oudheusden et al. (2008) for an infinite square prism revealed that the maximum turbulence intensity is located on the lateral sides while the maximum turbulence intensity for present work occurs in the shear layers separated from the leading edges (near the lateral sides) and behind the prism owing to the downwash flow.

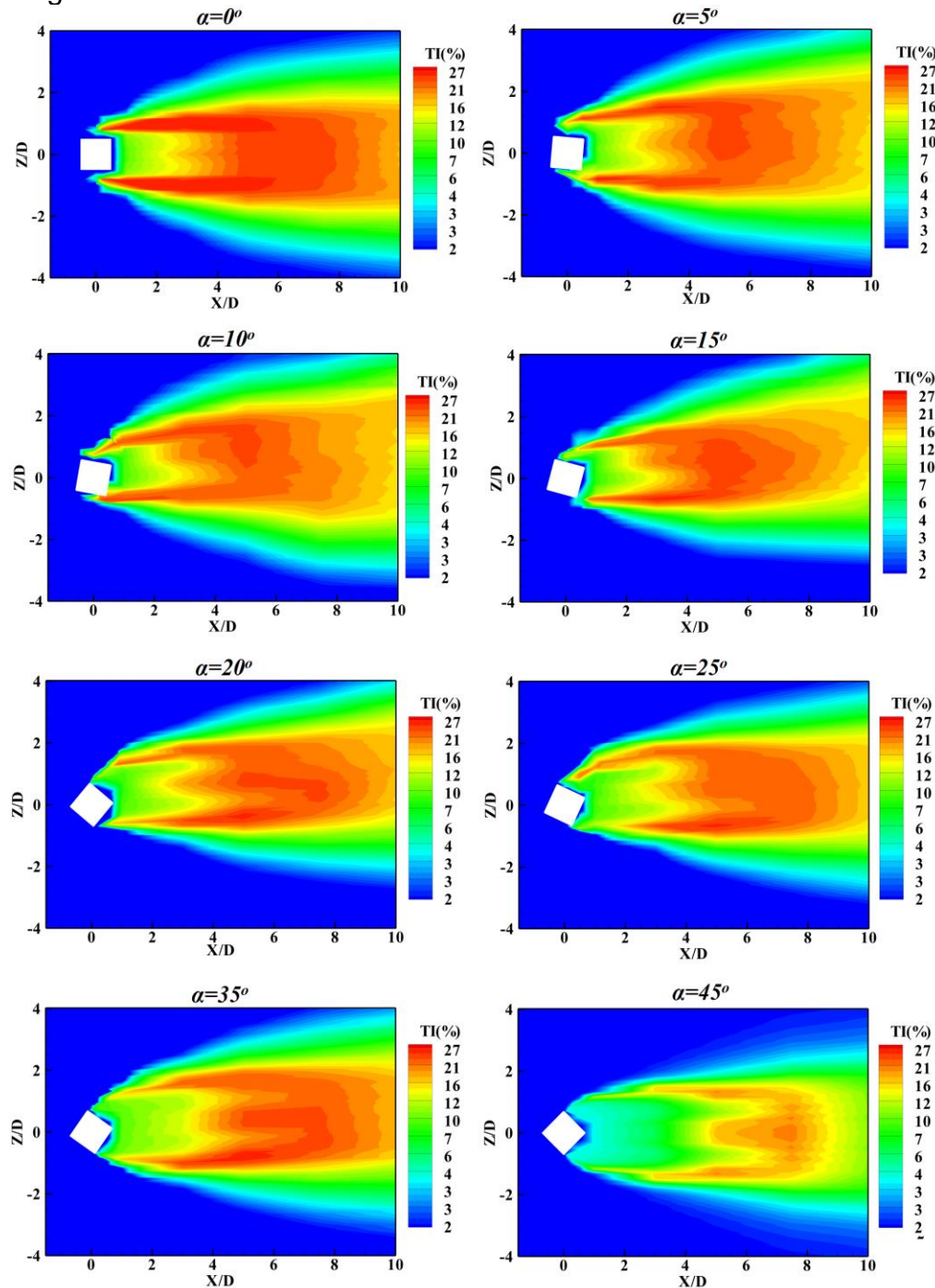


Fig. 7. Turbulence intensity contour at mid-height plane ( $Y/D=3.5$ ) for various incidence angles ( $Re=2 \times 10^4$ )

Fig. 8 indicates the turbulence intensity profiles for  $\alpha=0^\circ$ ,  $15^\circ$ ,  $45^\circ$  at  $Y/D = 3.5$  and  $X/D = 3, 5$ . Two peaks are observed on the shear layers at both  $X/D=3$  and 5 for all  $\alpha$  at  $1.5 < Z/D < 1.5$ . In addition, the turbulence intensity levels and its maximum decrease gradually by increasing the incidence angle so that the maximum turbulence intensity at  $\alpha=0^\circ$  and  $\alpha=45^\circ$  are 27% and 24%, respectively.

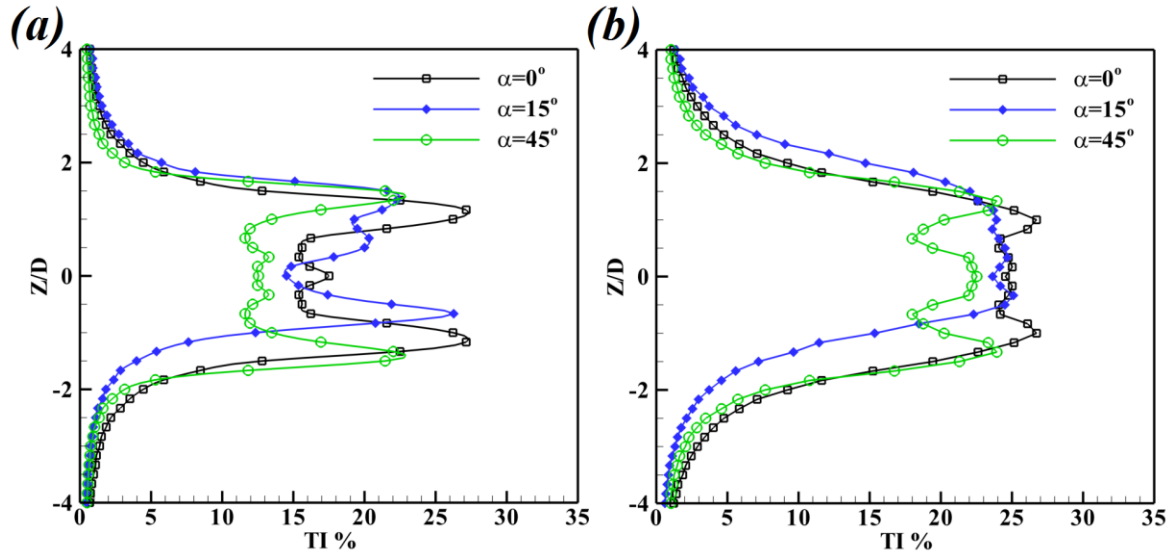


Fig. 8. Turbulence intensity profiles along the spanwise direction ( $Z$ ) at various angles at: (a)  $X/D=3$ , (b)  $X/D=5$ , ( $Y/D=3.5$  and  $Re=2 \times 10^4$ )

Fig. 9 shows the turbulence intensity on the  $X$ - $Y$  plane at  $Z/D=0$  for various  $\alpha$ . It should be noted that although Figs. 9 (b) and (c) provide a useful insight into the wake region, but it is expected that the contours shown in these figures could not present the thoroughgoing details of the flow field because of asymmetric structures at  $\alpha=15^\circ$  and  $25^\circ$ . As can be seen from Fig. 9 the turbulence intensity contours have two local maxima. The first one ranged from 19%-24% is located just on the shear layer above the free end surface and the other one ranged from 24%-27% is located behind the prism.

In order to make a detailed comparison between turbulence intensity distribution at different  $\alpha$ , the turbulence intensity profiles on the  $X$ - $Y$  plane at  $\alpha=0^\circ$  and  $45^\circ$  are provided in Fig. 10. It is seen from Figs. 9 and 10 that the location of the maximum turbulence intensity in the wake region moves farther downstream with increasing  $\alpha$ . For instance, the turbulence intensity reaches the peak values of 26% ( $\alpha=0^\circ$ ) at  $(X/D, Y/D) = (5, 4)$  and 24% ( $\alpha=45^\circ$ ) at  $(X/D, Y/D) = (7.5, 2.75)$ . It should be noted that at  $X/D=10$ , the turbulence intensity distribution at  $\alpha=0^\circ$  and  $45^\circ$  almost have a similar trend.

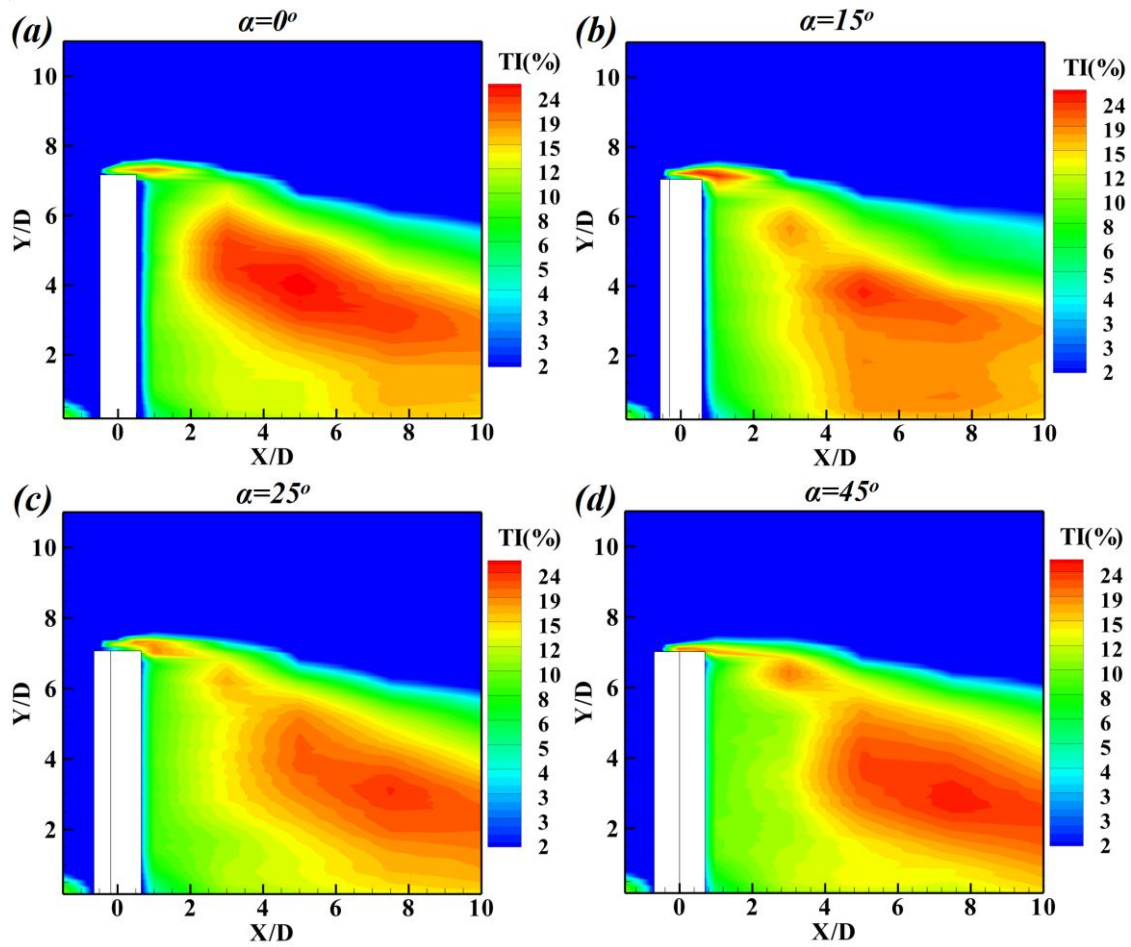


Fig. 9. Turbulence intensity contour on the X-Y plane at wake center plane ( $Z/D=0$ ),  $Re=2 \times 10^4$ . (a)  $\alpha = 0^\circ$ , (b)  $\alpha = 15^\circ$ , (c)  $\alpha = 25^\circ$ , (d)  $\alpha = 45^\circ$ .

The normalized wake width was determined by Huang et al. (2010) and Sohankar et al. (2015) for an infinite square cylinder at various incidence angles ( $Re=6776-77000$ ). In these works, the wake widths were measured at  $D/4$  and  $D$  downstream of the cylinder in Huang et al. (2010) and Sohankar et al. (2015), respectively. They illustrated that two local minimum wake widths occur at  $\alpha=0^\circ$  and  $15^\circ$ . At  $\alpha=0^\circ$  where the cross-stream width of the square cylinder has a minimum value, the local wake width is about  $1.25D$ , while it reaches to about  $1.2D$  at  $\alpha=15^\circ$  (Sohankar et al. 2015). The reduction of the wake width at the critical incidence angle ( $\alpha=15^\circ$ ) is due to the occurrence of the shear layer reattachment on the lower face (Sohankar et al. 2015). The shear layer passing closer to the body leads to a smaller the wake width. The maximum wake width occurs at  $\alpha=45^\circ$ , where it is about  $1.7D$ . If one scales the wake width with its projection width rather than  $D$  at each incidence angle, the normalized wake width is about 1.25, 0.98 and 1.21 for  $\alpha=0^\circ$ ,  $\alpha=15^\circ$  and  $\alpha=45^\circ$ , respectively (Sohankar et al. 2015).

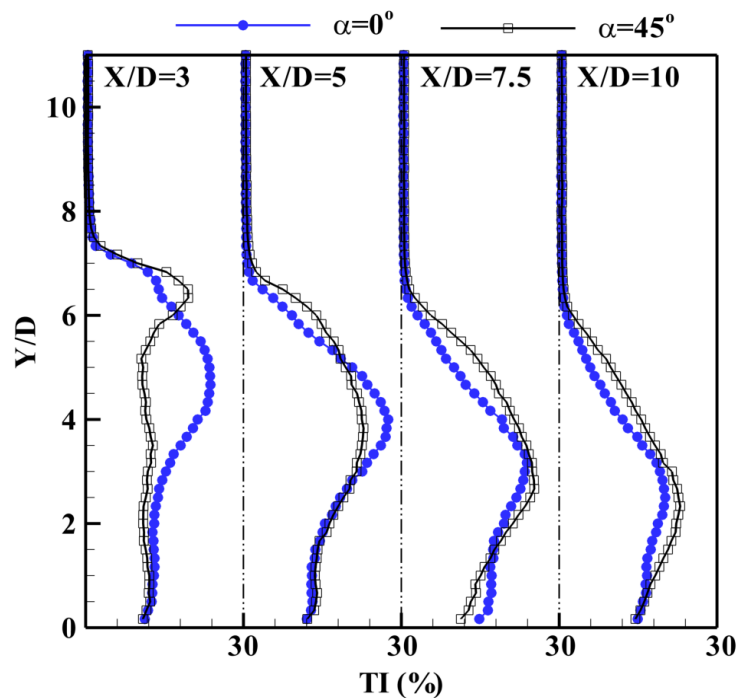


Fig.10. Turbulence intensity profiles on the X-Y plane at wake center plane ( $Z/D=0$ ) for  $X/D=3, 5, 7.5$  and  $10$  at  $\alpha=0^\circ, 45^\circ$  ( $Re=2 \times 10^4$ ).

In this study, the method employed by Huang et al. (2010) was used for estimation of the wake width for a finite prism. Huang et al (2010) for an infinite prism stated that the peak values on the turbulence intensity distributions were located in the shear layers. Therefore, the distance between these two peaks at each  $X/D$  could be used as an appropriate index for estimating the the wake width. It should be noted that the features of vortex formation and wake structure for a finite square cylinder are different from that of the infinite cylinder (Huang et al. 2010, Sohankar et al. 2015). Nevertheless, it is found some similarity between them, where the flow pattern in the middle of the finite prism should resemble the structure of an infinite cylinder due to a quasi-periodic shedding that is nominally parallel to the prism axis (Bourgeois et al. 2011). The scaled wake widths ( $W/D$ ) are shown for various incidence angles in Fig. 11 and compared with the results of Huang et al. (2010) and Sohankar et al. (2015). Despite the fact that the variation of the wake width of the finite square prism is not exactly identical to the infinite square prism, the minimum wake width occurs at the critical incidence angle ( $\alpha=15^\circ$ ) and the maximum value is present at  $\alpha=45^\circ$ . Furthermore, as can be seen at all incidence angles the wake width of the finite square prism is larger than the infinite one.



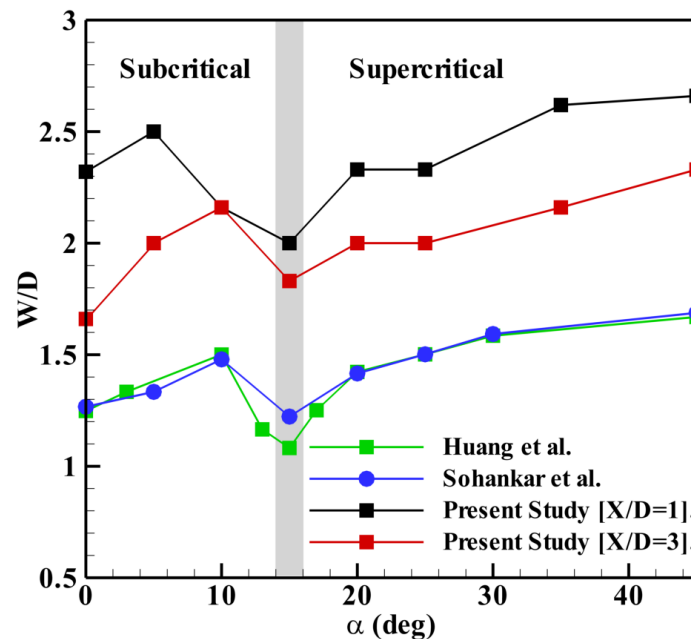


Fig. 11. Dependence of wake width (at  $Y/D=3.5$ ,  $X/D=1, 3$ ) on  $\alpha$  ( $Re=2 \times 10^4$ ). The results for the infinite cylinder are also included, where the wake width was measured at  $X/D=1/4$  and  $1.0$  in Huang et al. (2010) and Sohankar et al. (2015), respectively.

#### 4.2 Strouhal number

Fig. 12 presents the variation of  $St$  measured using a hotwire along the height of the finite square cylinder at three different streamwise locations for  $\alpha=0^\circ$ . The hot-wire probe was fixed at  $Z/D=2$  and it varies from  $Y/D=1$  to  $7$  for  $X/D=3, 5$  and  $10$ . The measurements were made at a freestream velocity of  $U_o=11$  m/s, corresponding to a  $Re=1.1 \times 10^4$ . The central frequency of the local maximum spectrum amplitude corresponds to the frequency of the vortex shedding.

The notable variations are observed in the shape and strength of the peaks in the power spectra along the height of the cylinder. Fig. 12 indicates that the amplitude of the dominant peak decreases near the free end, due to the interaction between downwash flow from the free end and spanwise vortex shedding as reported by Okamoto and Sunabashiri (1992).

Fig. 12 shows that  $St=0.107$  is dominant for the nine positions considered. Wang and Zhou (2009) also obtained identical power spectra at different streamwise locations. They stated that the major peak occurred at the same frequency throughout the cylinder span. This implies that the tip and base vortices may separate from the cylinder at the same frequency as spanwise vortices (Wang and Zhou 2009). McClean and Sumner (2014) used hot-wire measurements to see how the Strouhal numbers and power spectra changed along the height of square prisms with different  $AR$  and  $\alpha$ . They stated that for  $AR=11$  and  $\alpha=0^\circ$  a vortex shedding peak corresponding to  $St=0.10$  was detected along the entire height of the prism. Similar behavior was seen for  $\alpha=15^\circ$  where  $St=0.12$ , but the peaks tend to be wider than for  $\alpha=0^\circ$ . For  $AR=7$  and  $\alpha=0^\circ$ , the strong narrow vortex shedding peaks were found along the entire height of the prism.



For  $\alpha=15^\circ$ ,  $30^\circ$  and  $45^\circ$  the peaks were somewhat weaker near the ground plane and near the free end.

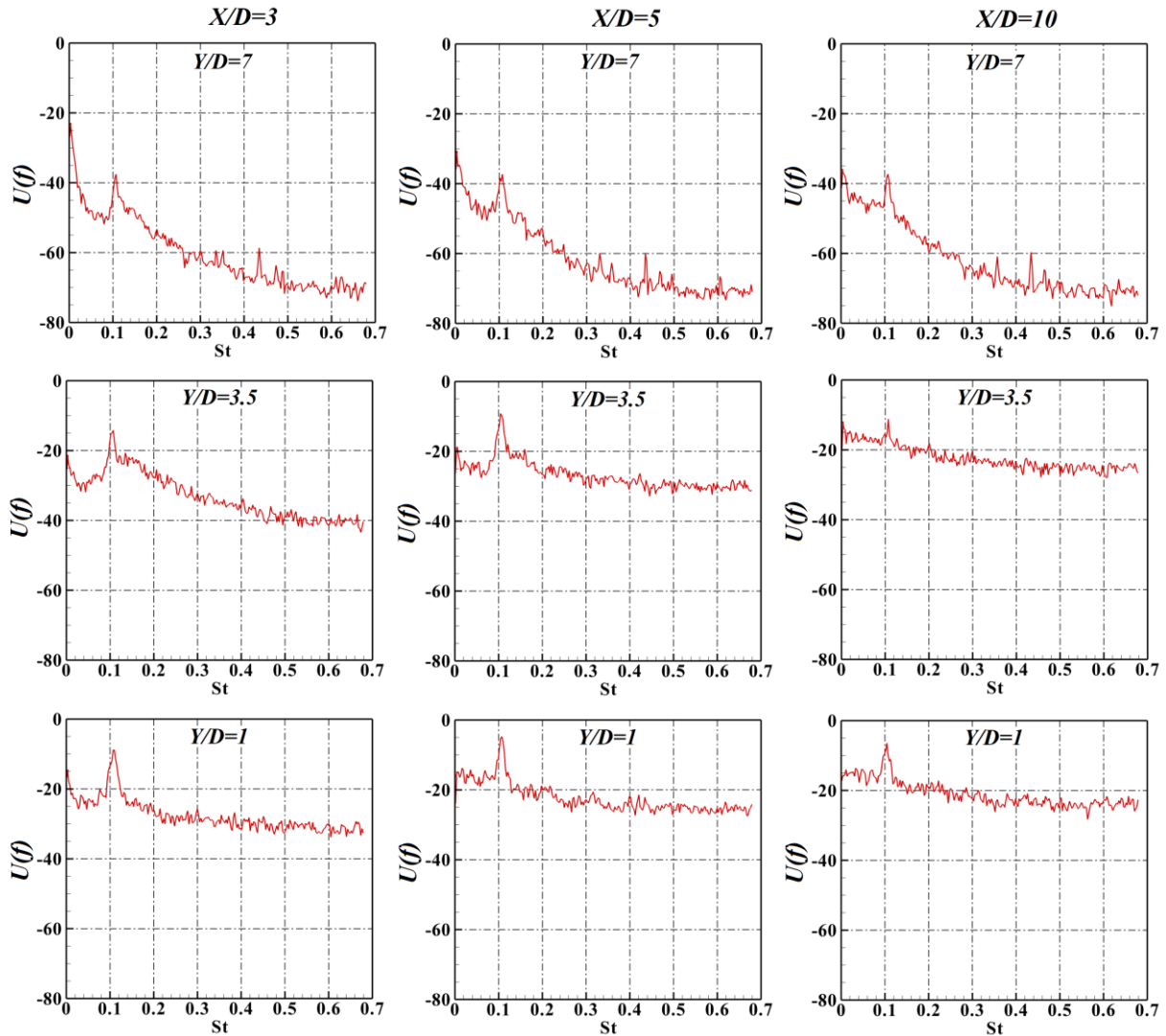


Fig. 12. Power spectra measured at various positions along the height ( $Y/D=1, 3.5, 7$ ) for  $X/D= 3, 5, 8$  at  $Z/D=2$  for  $\alpha=0^\circ$ ,  $Re=1.1 \times 10^4$ .

The  $St = 0.107$  in this work is lower than that of the infinite square cylinder, which was reported as  $0.125 \sim 0.13$  for  $Re=1 \times 10^3 \sim 2 \times 10^4$  (Okajima 1982). Zdravkovich (2003) attributed the decrease in the  $St$  of the finite-length cylinder to the free-end downwash flow. He suggested that the downwash flow elongates the vortex formation length and widens the near wake, thus prolonging the spanwise vortex shedding.

Fig. 13(a, b) indicates the frequency distributions of the vortex shedding obtained from the power spectrum density functions for  $0^\circ < \alpha < 45^\circ$  (with an increment of  $5^\circ$ ) at various free stream velocities from  $U=6.5$  m/s to  $28.5$  m/s ( $Re=6.5 \times 10^3 \sim 28.5 \times 10^3$ ). The hot-wire probe was installed in the downstream of the cylinder at  $X/D=5$ ,  $Y/D=3.5$  to obtain clear signals.

As seen from Fig. 13(a), the vortex shedding frequencies for all free stream velocities have similar variations with respect to the incidence angle. It is observed that

for each specific free stream velocity, the vortex shedding frequency increases slightly with increasing  $\alpha$ , reaching a maximum at  $\alpha=15^\circ$ , followed by a drop for subsequent rise in the incidence angle. The trend of the vortex shedding frequency of the present work is qualitatively similar with those reported by Huang et al. (2010) and Sohankar et al. (2015) for the infinite cylinder.

The previous research (Huang et al. (2010) and Sohankar et al. (2015), Rockwell 1977, Obasaju 1983) reported for an infinite cylinder that the occurrence of maximum  $St$  is related to the reattachment of the separated shear layer. The shear layer deflects at the reattachment point near the downstream corner of the cylinder and then rolls up at a distance downstream of the body to form a thin wake containing weaker vortices. The thin wake suggests a contraction of the distance between the shed vortices in both transverse and longitudinal directions. This also results in a higher shedding frequency.

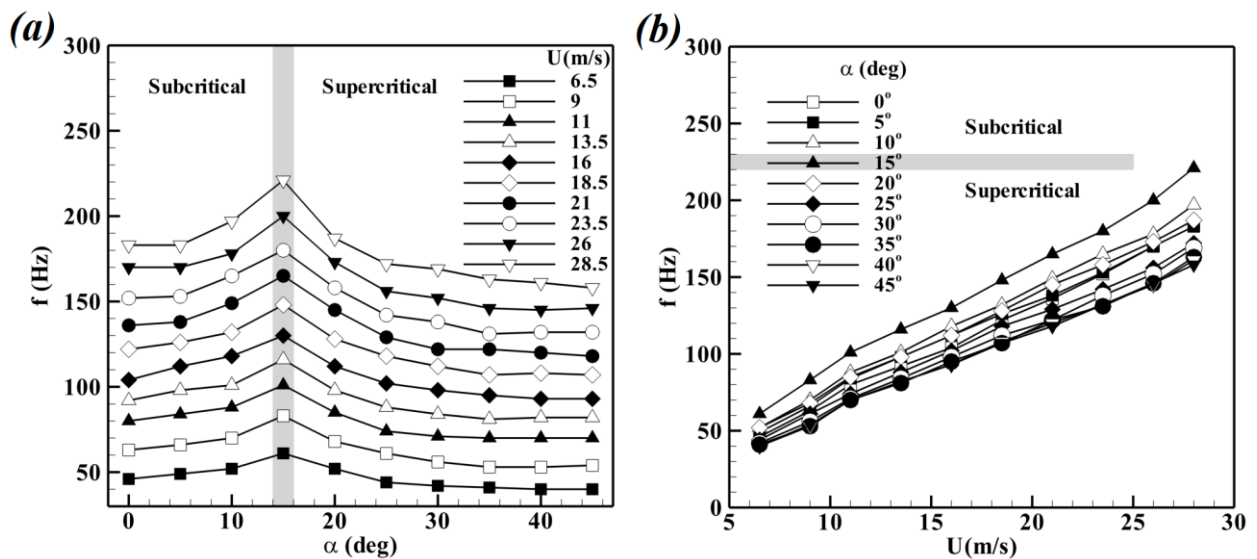


Fig.13. Variation of frequency with (a) incidence angle for various inflow velocities, (b) with inflow velocity for various incidence angles

Fig. 13(b) shows the variation of vortex shedding frequency with free stream velocity for various  $\alpha$ . It can be seen that for a specific  $\alpha$ , the vortex shedding frequency increases linearly with the increase of free stream velocity, regardless of subcritical or supercritical region. The vortex shedding frequency data presented in Fig.13 are converted to Strouhal numbers, i.e.  $St$  and  $St$  based on the cylinder side,  $D$ , and projected width of the cylinder on the cross-stream plane,  $D(\sin(\alpha)+\cos(\alpha))$ , respectively (Figs. 14). The use of projection width as the length scale for Strouhal number instead of the cylinder width is due to the conventional usage for non-circular objects, for instance, a flat plate, airfoil, oval, wedge, etc. (Huang et al. 2010 and Sohankar et al. 2015). In fact, the projection width shows approximately an order of the wake width of such bodies, which is an important flow parameter of the wake structure. In Fig. 14 (a, b), the results are plotted as functions of  $Re$  and  $\alpha$  and compared with the results of Huang et al. (2010) (an infinite square prism) and McClean and Sumner (2014) (a finite square prism with  $AR=7$ ). In Fig. 14 (c, d), the contours of  $St$  and  $St$  are provided for cases of Fig. 14(a, b), respectively.

Fig. 14 (a, c) shows that, for the infinite square prism, the Strouhal number is clearly sensitive to the incidence angle. Based on the results reported in the literature, the maximum  $St$  for a finite square cylinder occurs at  $\alpha_{cr} = 15^\circ - 17^\circ$  that is dependent on experimental conditions (McClellan and Sumner 2014). As shown in Fig.14 (a), the Strouhal number increases with increasing incidence angle from  $\alpha = 0^\circ$  to a maximum at  $\alpha = 15^\circ$ , followed by a gradual fall and then it approximately levels off for incidence angle greater than about  $30^\circ$ . The finite prism data of McClellan and Sumner (2014) for  $AR=7$  reveal that a maximum Strouhal number value occurs at  $\alpha=16^\circ$ , which is in good agreement with the present results. Fig. 14 (a) also shows the Strouhal numbers of the finite prism are higher than those of the infinite prism (Huang et al. 2010). Based on Fig. 14, the lowest value of Strouhal number occurs at  $\alpha=45^\circ$  or at  $\alpha=0^\circ$  when the side length (Fig. 14 (a)) or the projected width (Fig. 14 (b)) are used as the reference length scale, respectively. Fig. 14 also illustrates the Strouhal number slowly decreases as the  $Re$  increases. These differences become small for higher Reynolds numbers, where the  $St$  approximately approaches to same value for  $Re > 15 \times 10^3$ .

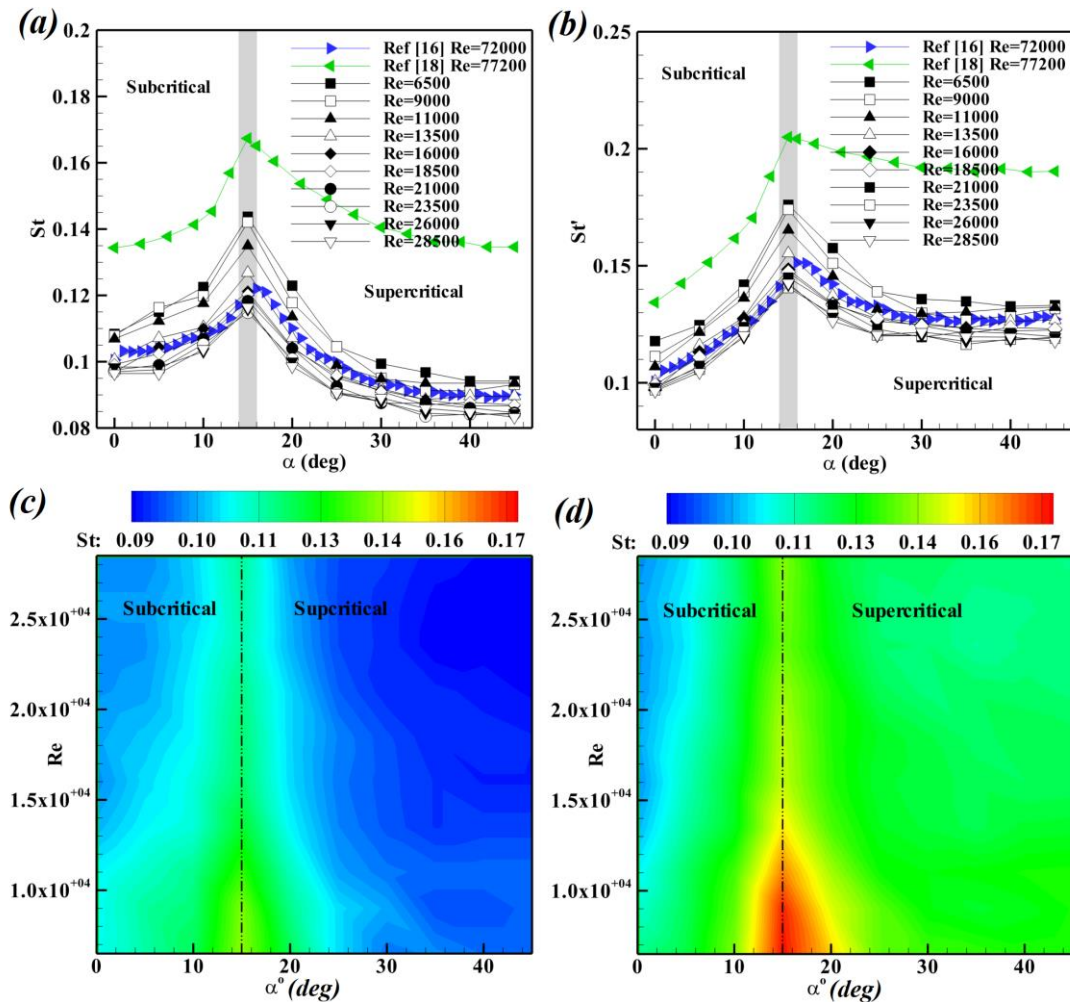


Fig. 14. Strouhal number based on (a, c) cylinder side  $D$ , and (b, d) projected width of the cylinder  $D(\sin \alpha + \cos \alpha)$ . The results of an infinite square prism (Huang et al. 2010) and a finite square prism (McClellan and Sumner 2014) are also included.

## 5. CONCLUSIONS

The experimental investigation of the flow field over a surface-mounted square prism is conducted. In particular, the effect of incidence angle on the wake structure and Strouhal number is addressed. The experiments are carried out in a low-speed wind tunnel at Reynolds numbers ranged from  $Re=6.5\times 10^3$  to  $28.5\times 10^3$  and for an aspect ratio of  $AR=7$  at incidence angles from  $\alpha=0^\circ$  to  $\alpha=45^\circ$ . The boundary layer is thin and its thickness relative to the prism height is  $\delta/H=0.07$ .

Regarding the wake structure, a downwash flow from the free end of the prism is observed. The downwash flow extends to the mid-height of the prism, resulting in the increase of velocity near the centerline. There is a reduction in the size of wake region along the height of square prism when moving away from the ground plane towards the free end. The reason for such behavior is due to the interaction between spanwise vortices, downwash and upwash flows in the downstream region of the cylinder. In addition, the wake width of the finite square prism changes with  $\alpha$ , a minimum wake width being at  $\alpha=15^\circ$  and a maximum wake width at  $\alpha = 45^\circ$ .

Similar to the infinite square prism the turbulence intensity distribution is sensitive to  $\alpha$ . In contrast to the infinite prism for which the maximum turbulence intensity occurs in the shear layers from the lateral sides, the maximum turbulence intensity for the finite square prism prevails in the shear layers separated from the free edge and behind the prism. This is generally attributed to the influence of the strong three-dimensional flow around the free end and to the downwash in the wake.

The results show that there is a dominant frequency for all positions considered and  $St$  along cylinder height has a constant value of 0.107 for  $\alpha = 0^\circ$ . The critical  $\alpha$  is found to  $15^\circ$  that separates the subcritical and supercritical regimes. The  $St$  reaches a maximum when the wake width is minimum. The physical reason for this phenomenon relates to the reattachment of the flow on the lateral side of the prism and the formation of the separation bubble.

There are some similarities between parameters of finite and infinite cylinders at incidence mostly in their trends, not values. For example, the trend of variations of frequency, Strouhal number and wake width are similar for both type of cylinders while their values are different. The angle at which the Strouhal number reaches a maximum value while the wake width has a minimum value is around  $15^\circ$  in finite and infinite cylinders. In addition, the wake width/Strouhal number of the finite square prism is larger/lower than that of the infinite cylinder for all incidence angles considered.

## REFERENCES

- Alam, M.M., Zhou, Y. and Wang, X.W. (2011), "The wake of two side-by-side square cylinders", *J. Fluid Mech.* **669**, 432–471.
- Alam, M.M., Bai, H.L., and Zhou, Y. (2016), "The wake of two staggered square cylinders", *J. Fluid Mech.* **801**, 475-507.
- Adaramola, M.S., Akinlade, O.G., Sumner, D., Bergstrom, D.J., and Schenstead, A.J. (2006), "Turbulent Wake of a Finite Circular Cylinder of Small Aspect Ratio", *J. Fluids Struct.* **22**, 919–928.
- Bourgeois, J. A., Sattari, P., and Martinuzzib, R. J. (2011), "Alternating half-loop shedding in the turbulent wake of a finite surface-mounted square cylinder with a thin boundary layer", *Phys. Fluids* **23**, 095101, 1-15.



- Brun, C., Aubrun S., Goossens, T., and Ravier, Ph.m. (2008), "Coherent structures and their frequency signature in the separated shear layer on the sides of a square cylinder", *J. Flow, Turb. Comb.* **81**, 97–114.
- Chen, J.M., Liu, C.H. (1999), "Vortex shedding and surface pressures on a square cylinder at Incidence to a uniform Air Stream", *J. Heat Fluid Flow* **20**, 592–597.
- Dutta, S., Muralidhar, K., and Panigrahi, P.P. (2003), "Influence of the orientation of a square cylinder on the wake properties", *Exp. Fluids* **34**, 16-23.
- Huang, R. F., Lin, B. H., and Yen, S. C. (2010), "Time-averaged topological flow patterns and their Influence on vortex shedding of a square cylinder in cross flow at Incidence", *J. Fluids Struct.* **26**, 406–429.
- Igarashi, T. (1984), "Characteristics of the flow around a square prism", *Bull. JSME* **27**, 1858-1865.
- Jorgenson, F. (2002) "How to Measure Turbulence with Hot-wire Anemometers" (A Practical Guide), Dantec Dynamics, Skovlunde, Denmark.
- Lee, B.E. (1975) "The effect of turbulence on the surface pressure field of a square prism", *J. Fluid Mech.* **69**, 263-282.
- Lyn, D.A., Einav, S., Rodi, W., and Park, J.H. (1995), "A laser-Doppler velocimetry study of ensemble-averaged characteristics of the turbulent near wake of a square cylinder", *J. Fluid Mech.* **304**, 285-319.
- McClellan, J. F., Sumner. D. (2014), "An experimental investigation of aspect ratio and incidence angle effects for the flow around surface-mounted finite-height square prisms", *J. Fluids Eng.* **136**, 081206, 1-10.
- Minguez, M., Brun, C., Pasquetti, R., and Serre, E. (2011), "Experimental and high order LES analysis of the near wall flow over a square cylinder", *J. Heat Fluid Flow* **32**, 558-566.
- Norberg, C. (1993), "Flow around rectangular cylinders: Pressure forces and wake frequencies", *J. Wind Eng. Indust. Aerodyn.* **49**, 187-196.
- Obasaju, E.D. (1983), "An investigation of the effects of incidence on the flow around a square section cylinder", *Journal of Aeronaut Quarterly*, **34**, 243-259.
- Okajima, A. (1982), "Strouhal Numbers of Rectangular Cylinders", *J. Fluid Mech.* **123**, 379–398.
- Okamoto, H., Sunabashiri, Y. (1992), "Vortex Shedding from a Circular Cylinder of Finite Length Placed on a Ground Plane", *J. Fluids Eng.* **114** (4), 512-521.
- Oudheusden, B.W., Scarano, F., Hinsberg, N.P., and Roosenboom, E.W.M. (2008), "Quantitative visualization of the flow around a square-section cylinder at incidence", *J. Wind Eng. Indust. Aerodyn.* **96**, 913-922.
- Park, C.W., Lee, S.J. (2000), "Free end Effects on the Near Wake Flow Structure behind a Finite Circular Cylinder", *J. Wind Eng. Indust. Aerodyn.* **88**, 231- 246.
- Rockwell, D.O. (1977), "Organized fluctuations due to flow past a square cross section cylinder", *J. Fluids Eng.* **99**, 511-516.
- Saha, A. K. (2013), "Unsteady flow past a finite square cylinder mounted on a wall at low Reynolds number", *Comp. Fluids* **88**, 599-615.
- Sakamoto, H., Arie, M. (1983), "Vortex Shedding from a Rectangular Prism and a Circular Cylinder Placed Vertically in a Turbulent Boundary Layer", *J. Fluid Mech.* **126**, 147-165.

- Sakamoto, H. (1985), "Aerodynamic Forces Acting on a Rectangular Prism Placed Vertically in a Turbulent Boundary Layer", *J. Wind Eng. Indust. Aerodyn.* **18**, 131–151.
- Sarode, R.S., Gai, S.L., and Ramesh, C.K. (1981), "Flow around circular- and square-section models of finite height in a turbulent shear flow", *J. Wind Eng. Indust. Aerodyn.* **8**, 223-230.
- Sohankar, A., Norberg, C. and Davidson, L. (1999), "Simulation of unsteady 3D flow around a square cylinder at moderate Reynolds number", *Phys. Fluids* **11**, 288-306.
- Sohankar, A., Davidson, L., and Norbeg, C. (2000), "Large eddy simulation of flow past a square cylinder: comparison of different subgrid scale models", *J. Fluids Eng.* **122**, 39-47.
- Sohankar, A. (2006), "Flow over a bluff body from moderate to high Reynolds numbers using large eddy simulation", *Comp. Fluids* **35**, 1154-1168.
- Sohankar, A. (2008), "Large eddy simulation of flow past rectangular section cylinders: side ratio effects", *J. Wind Eng. Indust. Aerodyn.* **96**, 640-655.
- Sohankar, A., Mohagheghian, S., Dehghan, A.A., and Dehghan Manshadi, M. (2015), "A smoke visualization study of the flow over a square cylinder at incidence and tandem square cylinders", *J. Visualization* **18**, 687-703.
- Sumner, D., Heseltine, J.L., and Dansereau, O.J.P. (2004), "Wake structure of a finite circular cylinder of small aspect ratio", *Exp. Fluids* **37**, 720-730.
- Trias, F. X. Gorobets, A. and Oliva A. (2015). "Turbulent flow around a square cylinder at Reynolds number 22,000: A DNS study", *Comp. Fluids* **123** (22), 87–98.
- Wang, H.F., Zhou, Y., Chan, C.K., Wong, W.O., and Lam., K.S. (2004) "Flow Structure around A Finite Length Square Prism", *15th Australasian Fluid Mechanics Conference*, The University of Sydney, Sydney, Australia.
- Wang, Y., Zhou, C.K., Chan and Lam., K.S. (2006), "Effect of Initial Conditions on Interaction between a Boundary Layer and a Wall-Mounted Finite-Length-Cylinder Wake", *Phys. Fluids* **18**, 065106, 1-12.
- Wang, H.F., Zhou, Y. (2009), "The finite-length square cylinder near wake", *J. Fluid Mech.* **638**, 453–490.
- West, G.S., Apelt, C.J. (1982), "The effects of tunnel blockage and aspect ratio on the mean flow past a circular cylinder with Reynolds numbers between  $10^4$  and  $10^5$ ", *J. Fluid Mech.* **114**, 361–377.
- Williamson C.H.K. (1996), "Three-dimensional wake transition", *J. Fluid Mech.* **328**, 345-407.
- Yavuzkurt, S. (1984), "A guide to uncertainty analysis of hot-wire data", *J. Fluids Eng.* **106**, 181-186.
- Yen, S.C., and Yang, C.W. (2011), "Flow patterns and vortex shedding behavior behind a square cylinder", *J. Wind Eng. Indust. Aerodyn.* **99**, 868-878.
- Yen, S.C., Yang, C.W. (2012), "Characteristic Flow Field Behind a Square-Cylinder Using Upstream Mesh Fences", *J. Fluids Eng.* **134**, 091202-1-9.
- Zdravkovich, M.M. (2003), "Flow around circular cylinders", Vol. 2: Applications. Oxford University Press.
- Zheng, Q., and Alam, M.M. (2017), "Intrinsic features of flow past three square prisms in side-by-side arrangement", *J. Fluid Mech.* (in press).